Materials Physics and Mechanics. 2023;51(4): 172-185
Research article
http://dx.doi.org/10.18149/MPM.5142023_15

Submitted: November 10, 2022
Approved: March 20, 2023
Accepted: April 26, 2023

Ab initio study of Hydrogen and Lithium behaviors in Cu_2O

A. Larabi [1], M. Mebarki [1] ✉, I. Abdellaoui [2],

A. Mahmoudi [3], S. Merazga [1], N. Gabouze [1]

[1] Centre de Recherche en Technologie des Semi-conducteurs pour l'Energétique (CRTSE), Alger, Algeria

[2] The Center for the Development of Advanced Technologies, Alger, Algeria

[3] Université Abou Bekr Belkaid Tlemcen, Tlemcen, Algeria

✉ Mebarki.Mourad@crtse.dz

Abstract. Nowadays, produced green energy requires efficient storage, the materials to be used must be at unbeatable prices. Lithium and hydrogen are two candidates in several applications in the field of renewable energies. The effect of Hydrogen or Lithium on the electronic, magnetic and optical properties of cuprous oxide Cu_2O has been investigated using the projected augmented wave (PAW) based on the density functional theory (DFT) formalism, within the generalized gradient approximation (GGA). Different concentrations of hydrogen and lithium were taken into consideration. The calculated formation energies indicate that the H-Cu_2O system is stable for all hydrogen concentrations. The density of electronic states calculations show that Cu_2O is p-type and it keeps the same type after hydrogen or lithium incorporation. The correlation of the obtained results gives us more precision on the physical properties of H or Li: Cu_2O.
Keywords: Cu_2O; Hydrogen; Lithium; energy storage; DFT

Acknowledgements. *This work was funded under the Algerian General Directorate of Scientific Research and Technological Development (DGRSDT). The authors are grateful to Professor Abdelhamid Layadi, L.E.S.I.M.S., Département de Physique, Université Ferhat Abbas, Setif 1, Algeria, for helpful suggestions.*

Citation: Larabi A, Mebarki M, Abdellaoui I, Mahmoudi A, Merazga S, Gabouze N. Ab initio study of Hydrogen and Lithium behaviors in Cu_2O. *Materials Physics and Mechanics*. 2023;51(4): 172-185. DOI: 10.18149/MPM.5142023_15.

Introduction

The evolution of the performance of innovative batteries has played an important role in the energy research community since its beginning. Consequently, it is essential to study excellent materials for applications in advanced batteries of electric vehicles, hybrid electric vehicles and energy storage. The various materials used in lithium battery electrodes are selected for their best performance in cyclability and their high specific capacities. Several studies have been made to come out and test the ability to use cuprous oxides as electrodes in lithium batteries [1–5]. Several candidates, such as cuprous oxide (Cu_2O) with a theoretical capacity of 375 mA h/g, have attracted more interest due to their high abundance, low production cost and nontoxic nature [6–8]. The Cu_2O nanostructures with varied morphology, such as cubic, star-shaped crystalline particles [9] and nanowires [10] have a big impact on the enhancement of

Publisher: Peter the Great St. Petersburg Polytechnic University

the specific capacity and the cycling capability for lithium-ion batteries (LIBs) and Hydrogen storage.

Up to now, several scientific efforts have been focused on the study of the physical properties of Cu_2O and these different applications. The electronic and photocatalytic properties of Cu_2O with different Mn concentrations and configurations have been investigated by the density functional theory (DFT) [11]. The GGA and GGA + U approaches were applied to obtain the Cu_2O band structures and thermoelectric properties [12]. The examination of the halogens doping effects of Cu_2O has been reported in the literature [13]; this was done by using first-principle calculations of the electronic structures and the optical properties. The effect of Li doped Cu_2O has been investigated by Nyborg et al. [14,15]. Yifei et al. demonstrated the feasibility of the successive "conversion-deposition" mechanism for realizing long-cycle-life composite Li anode, thus after insertion of Li ion into Cu_2O and deposited in the form of Li metal at successive low potential [16]. Cu_2O nanowire arrays has been used to provide a new strategy to high performance Li metal battery based on 3d conductive skeleton with lithiophilic [17]. In the other hand, Xue Zhou et al. proposed a new strategy to protect Cu_2O hydrogen-substituted graphdiyne [18]. The hydrogenation strategy is employed, also, to improve sensing performances of Cu_2O [19].

In this work, the first principles calculations were used to study the substitutional hydrogen and lithium effect on the electronic, magnetic and optical properties of Cu_2O. To verify the system stability in presence of hydrogen or lithium, we calculated the formation energies of different proposed concentrations. In addition, the influence of hydrogen and lithium on the physical properties Cu_2O is investigated. We also predict and give an easy, low-cost and scalable strategy to prepare the Cu_2O for energy storage.

Method

We used ab initio total-energy and molecular-dynamics program VASP (Vienna ab initio simulation program) developed at the Fakultät für Physik of the Universität Wien [20,21]. For the exchange and correlation energies treatment, we adopted the generalized gradient approximation (GGA) [22] with projector-augmented wave (PAW) [21,23] pseudo-potentials. Brillouin zone integrals converged with a 450 eV plane-wave cut-off and a $2 \times 2 \times 2$ Monkhorst-Pack k-point mesh, sufficient to insure the energy convergence for the supercell. These calculations showed a discrepancy within 10^{-7} eV. We relaxed the structure with the standard conjugated gradient algorithm. We used the supercell approach to simulate the H or Li doped Cu_2O system. The optimized lattice constant of Cu_2O is a = 4.14 Å which is in good agreement with the experimental value of a = 4.27 Å [24,25] and theoretical values a= 4.18 and 4.20 Å [26,27].

In these calculations, we positioned the H and Li atoms at the cation sites (Cu). We performed the hydrogen and lithium formation energies calculations on $3 \times 3 \times 3$ supercell with 162 atoms (Fig. 1), using the calculated lattice constant with the different concentrations in the cell. The supercell size is necessary for a detailed study of many dopant geometric structures. For calculations of the electronic properties of H or Li doped Cu_2O, we suppose that H and Li atoms lead to form a $3 \times 3 \times 3$ supercell with chemical composition $Cu_{2(108-x)}H_xO_{54}$ or $Cu_{2(108-x)}Li_xO_{54}$ with different atoms of hydrogen or lithium at the substitutional sites. The calculations were spin-polarized.

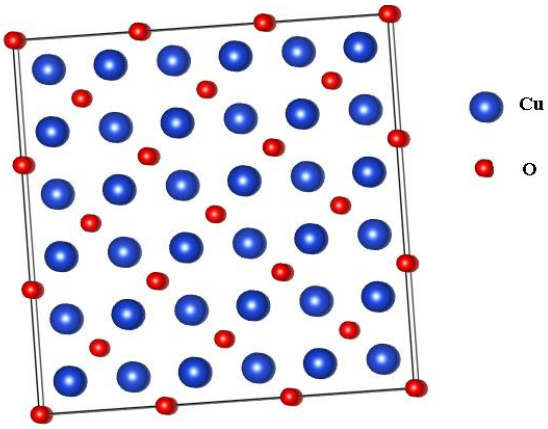

Fig 1. Supercell of 3 × 3 × 3 Cu_2O lattice with 162 atoms

Optical properties can be determined using the complex dielectric function $\varepsilon(\omega)=\varepsilon_1(\omega)+i\varepsilon_2(\omega)$ [28]. The imaginary part of the dielectric function $\varepsilon_2(\omega)$ was calculated from the momentum matrix elements between the occupied and unoccupied wave functions [29]:

$$\alpha(\omega) = \sqrt{2}\left(\frac{\omega}{c}\right)\left[\sqrt{\varepsilon_1^2(\omega) - \varepsilon_2^2(\omega)} - \varepsilon_1(\omega)\right]^{\frac{1}{2}}. \quad (1)$$

Results and discussion

Structures and formation energies. In order to confirm the stability of the system in the presence of hydrogen or lithium, we calculate the formation energies for different concentrations of Hydrogen and Lithium in Cu_2O. The refs. [30–32] give the formation energy for hydrogen in Cu_2O as:

$$E_f = E_{\mathrm{Cu2O}+H} - E_{\mathrm{Cu2O}} - nE_{tot}^{H} + nE_{tot}^{Cu} + qE_F. \quad (2)$$

The formation energy for lithium in the Cu_2O is given by:

$$E_f = E_{\mathrm{Cu2O}+Li} - E_{\mathrm{Cu2O}} - nE_{tot}^{Li} + nE_{tot}^{Cu} + qE_F, \quad (3)$$

where $E_{\mathrm{Cu2O}+H}$ and $E_{\mathrm{Cu2O}+Li}$ are the total energy of the supercell with hydrogen and lithium respectively; $E_{\mathrm{Cu2O}}$is the total energy of the supercell without hydrogen or lithium. The ground state total energies, E_{tot}^{H}, E_{tot}^{Cu} and E_{tot}^{Li} correspond, respectively, to isolated hydrogen, cuprous and lithium atoms; n denotes the number of H or Li atoms introduced in Cu_2O system. The last term in the formation energy accounts for the fact that H^+ or Li^+ donates an electron and H^- or Li^- accepts an electron. E_F is the Fermi level energy. If the formation energy is negative ($E_f < 0$), the implantation of the hydrogen or lithium atom into the Cu_2O lattice is energetically favorable.

In the Fig. 2(a), we present the variation of the calculated formation energies with the hydrogen concentration. We can see that all calculated formation energies are negative which indicate the stability of Cu_2O in presence of hydrogen. Figure 2(b) shows the formation energy values for different Li concentrations. The formation energies of the first two lithium concentrations are positive. Thus, the system is not stable, which is probably due to the possible formation of Li_2O, this case is reported in the literature [33]. Beyond the two first concentrations, the values of all formation energies become negative and decrease in a linear way with a low slope, this state is more stable and opens the possible feasibility to the experimentation of Li: Cu_2O [34].

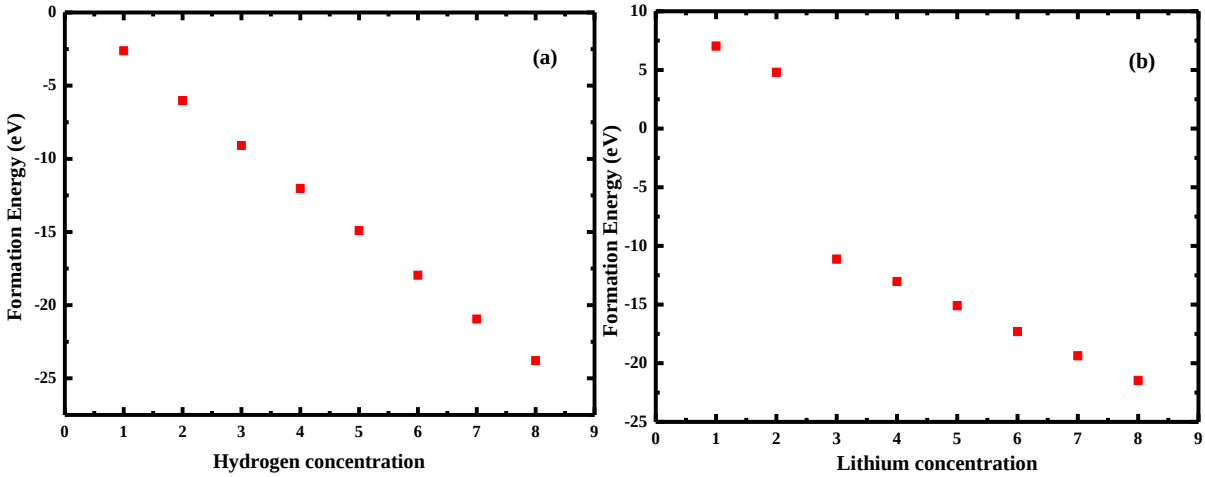

(a) (b)

Fig. 2. Formation energy variation with Hydrogen (a) and Lithium(b) concentration

Table 1. System energies, bond lengths (Å), band-gaps and Fermi levels energies in the undoped, H and Li-doped Cu_2O systems calculated using GGA-PBE

System	Energies	E_g(eV)	E_F(eV)	Cu-Cu	Cu-O	Cu-dopant	O-dopant
Undoped	-739.09	0.55	3.236	2.931	1.794	-	-
1H	-741.67	0.42	2.177	3.037	1.86	2.678	1.198
2H	-741.85	0.32	2.232	3.022	1.865	2.82	1.097
3H	-742.09	0.32	2.299	3.126	1.864	2.697	1.195
4H	-742.26	0.43	2.283	3.003	1.858	2.557	1.078
5H	-742.34	0.43	2.312	3.004	1.873	2.663	1.049
6H	-742.66	0.43	2.302	3.006	1.856	2.521	1.054
7H	-742.8	0.43	2.296	3.009	1.864	2.512	1.046
8H	-742.95	0.43	2.392	3.005	1.848	2.505	1.062
1Li	-726.98	0.66	3.355	2.915	1.785	2.872	1.658
2Li	-727.32	0.66	3.356	2.918	1.787	2.863	1.673
3Li	-742.53	0.42	2.139	3.039	1.857	3.015	1.797
4Li	-742.54	0.52	2.219	3.002	1.861	2.981	1.741
5Li	-742.83	0.52	2.232	3.025	1.86	3.01	1.744
6Li	-743.09	0.52	2.135	2.995	1.848	2.972	1.74
7Li	-743.44	0.52	2.138	3.037	1.863	2.991	1.749
8Li	-743.74	0.52	2.104	3.006	1.86	2.992	1.749

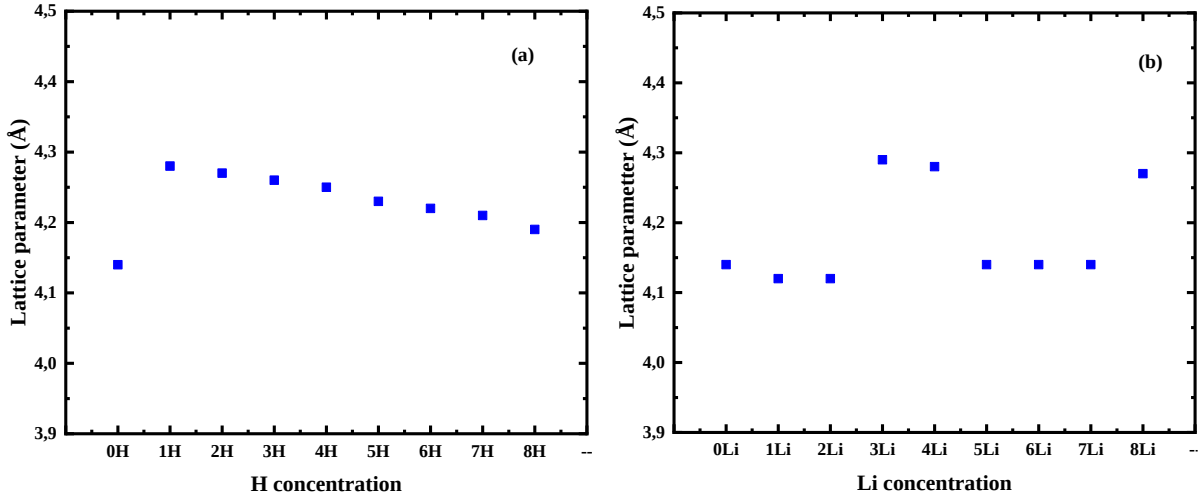

(a) (b)

Fig. 3. Lattice parameter variation with Hydrogen (a) and Lithium (b) concentrations

Magnetic and electronic properties. From the densities of states (see Figs. 4 and 5), we note that, for all concentrations (of H or Li), the difference between the majority and minority densities of states near the Fermi energy is equal to zero. This indicates that the presence of substitutional hydrogen or lithium does not generate a magnetic moment order in Cu_2O. The calculated band gap of undoped Cu_2O is about 0.55 eV, which is smaller than the experimental value (2.17 eV) [35] but it agrees well with the previous theoretical value reported in literature (0.6 eV [36,37], 0.64 eV [38] and 0.7 eV [39].

The density of states (DOS) for Cu_2O is calculated in order to understand the electronic structure and nature of the band edge wave functions (see Fig. 6). The projected DOS clearly shows significant *p-d* (O-2*p* and Cu-3*d*) hybridization below Fermi level, with Cu-3*d* bands dominating the valence and the conduction band edge. From this, it is clear that the interaction between metal-metal, which is controlled by the interatomic distances Cu-Cu, defined the band gap energy.

The calculated band gap energies for different concentrations of dopants in Cu_2O are shown in Fig. 7. The decrease in energy values of the Fermi level indicates that the doped system is a degenerate p-type semiconductor, as seen in Table 1. The total and partial DOS of H-*1s*, Li-*2s*, O-*2p* and Cu-*3d* states are plotted in Figs. 8 and 9(b,c). The dopant contribution to the calculated DOS is at low energy level, no dopants bands in the top VB or in the bottom of CB are observed, where the band edge of doped Cu_2O have the same features as pure system. For H-doping, the sharp peak at -5.5 eV corresponds to the fully symmetric orbital of the hydrogen multicenter bond in Cu_2O [40]. Clearly, it shows strong localized energy bands, which is from O-*2p*, Cu-*4s* and H-1*s* states. The sharp peak at -2 eV shows strong coupling between Cu-3*d* and H-1*s* states. Moreover, the states close to the VBM (-2 to 0 eV) are dominated by Cu-3*d* and O-2*p* hybrid orbitals. Beyond the CBM, the Cu and H bands are resonant and strongly mix with the host CB states. For Li-doping, the sharp peaks at -6.5 show strong localized energy bands from O-2*p* states and Li-*2s* states without the presence of the Li-2*s* bands near Fermi level and contribution of Cu-*4s* orbitals considering the H-doping system. The energy bands of the doped system are deeper than that of the undoped system. It can be explained by the strong bonding of substitution atoms with their neighbors compared to Cu atoms. They are further stabilized systems as showing the lower energetic values (see Table 1).

It is known that in the case of doping, the filling effect of the band edge near the Fermi level cannot be ignored. In this context, we analyzed the charge transfer based on Bader's theory. The absolute value of charge transfer of undoped and doped Cu_2O is shown in Fig. 10, which characterizes the ability of atoms to gain and lose electrons. In the case of an undoped system, the cation Cu atom loses electrons and the anion O atom gains electrons. In doped systems, H atoms are considered donors because they undergo negative charge transfer. Therefore, it is slightly changed compared to an undoped system where O atoms receive charges from Cu and H atoms. The charge loss of Cu in the H-doped system is slightly less than that of the undoped system. This shows that the sharing of charge between H+ and O atoms results in the formation of a typical H-O covalent bond, which leads to a decrease in the electronegativity of the O atom and an increase in the strength of the copper-copper covalent bond. This reduces the ionicity of the Cu-O bond and clarifies the peak intensity in DOS. Due to the reduced hybridization between Cu and O atoms, the peak intensity after doping is very weak. In addition, we can see that despite the covalent increase due to the O-H bond, the band gap shrinkage rate is limited to 0.32 eV, with no significant changes in structural distortion and electronic structure.

For Li-doped Cu_2O, we can see that 1Li and 2Li doping increase the band gap. This can be explained by reducing the copper spacing, which increases the Cu-*3d* band overlap, as listed in Table 1. For the charge transfer from the cation to the anion atom, there is no significant change compared to the undoped system. However, as shown in Table 1, due to the increase in

ion characteristics, 3-8Li doping reduces the band gap less than the H doping case. We can see that there is no important modification in the band gap value in the case of high concentration Li-doping, this result agree with previous work [14]. It can be seen that the band gap changes of the two dopants are the result of the simultaneous filling effects: the Cu-*3d* band and the orbital-lattice coupling.

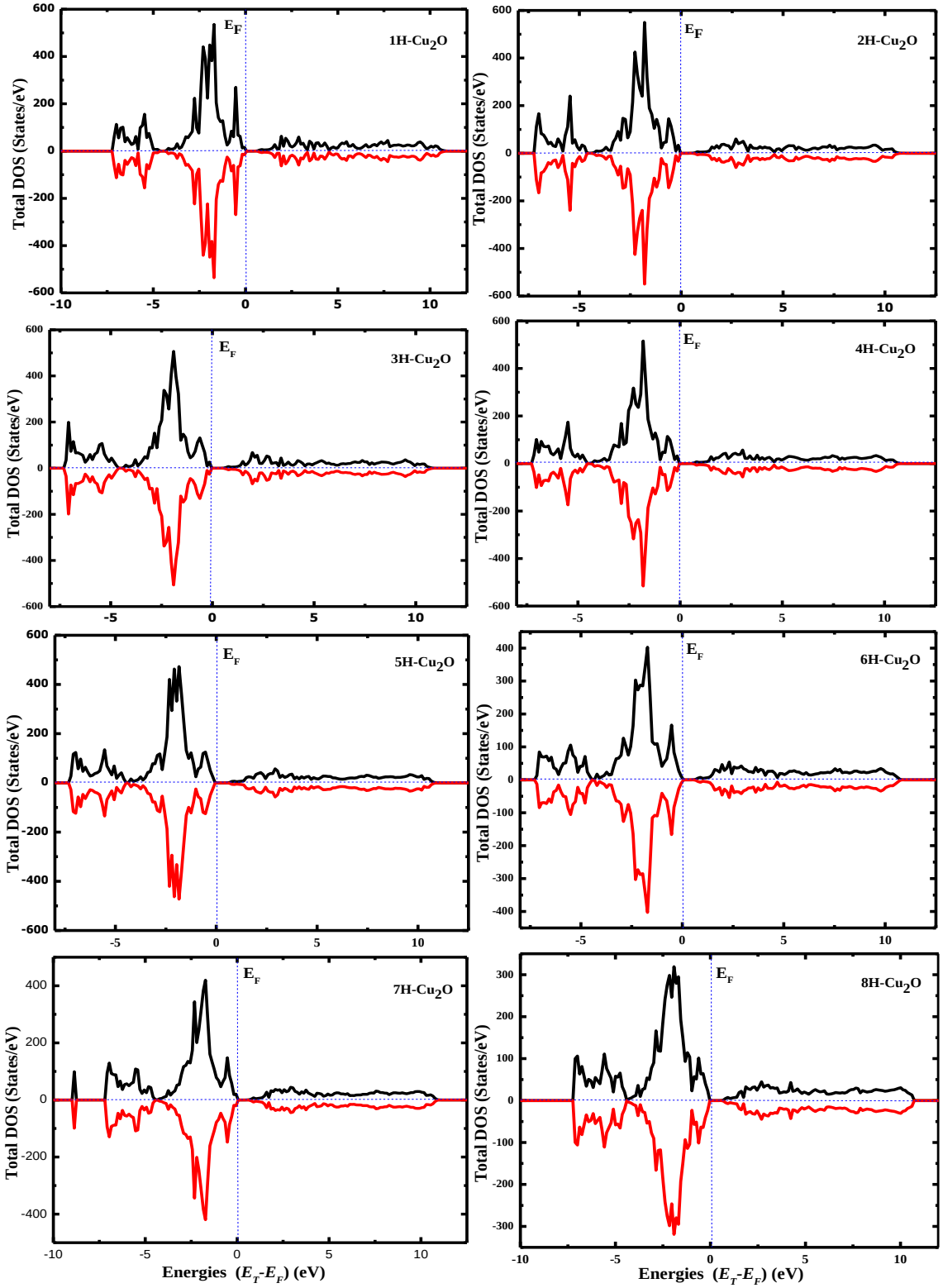

Fig. 4. Calculated density of states of H-Cu_2O for different concentrations of hydrogen. Dashed line is the Fermi level E_F

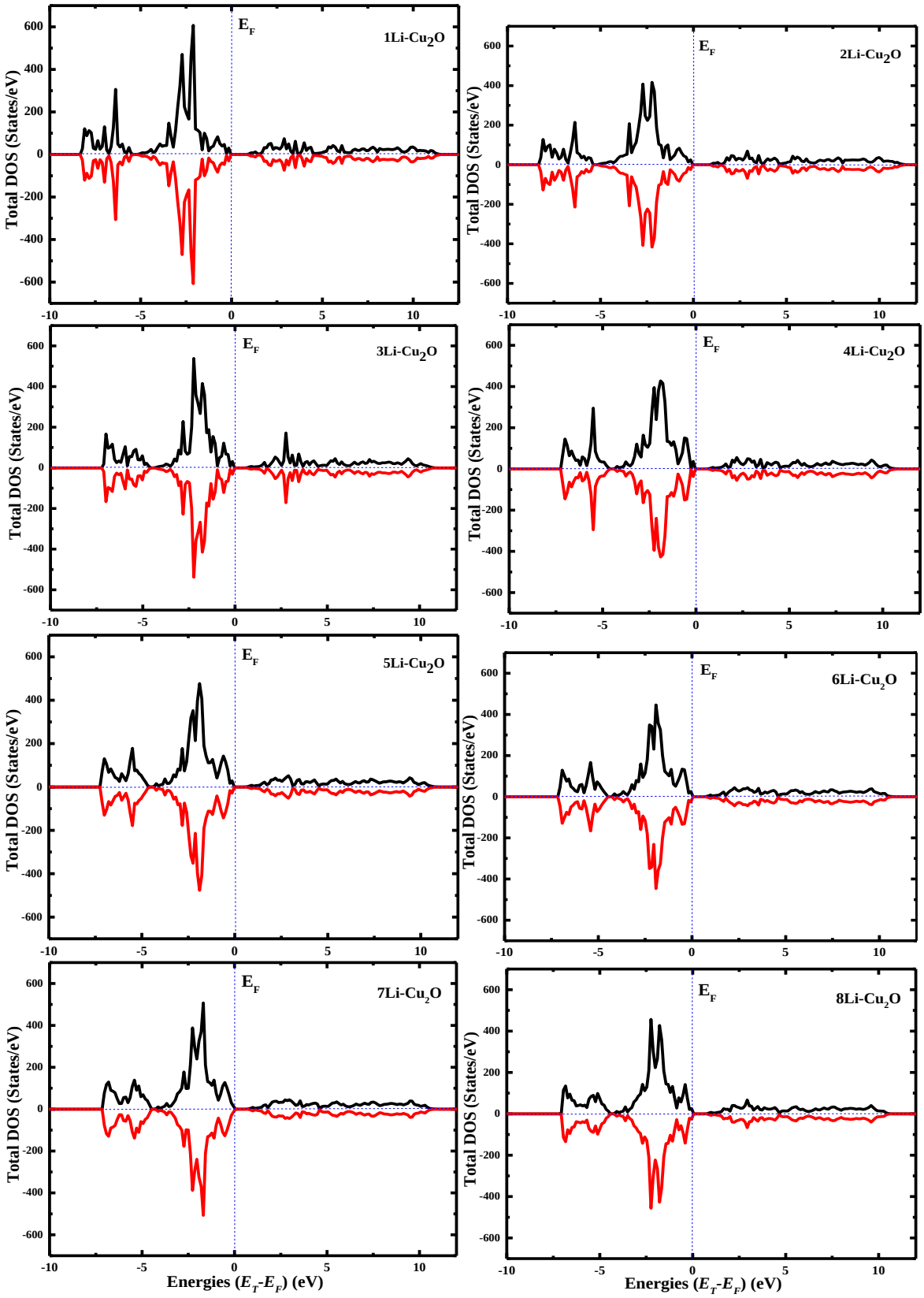

Fig. 5. Calculated density of states of Li-Cu_2O for different concentrations of lithium. Dashed lines is the Fermi level E_F

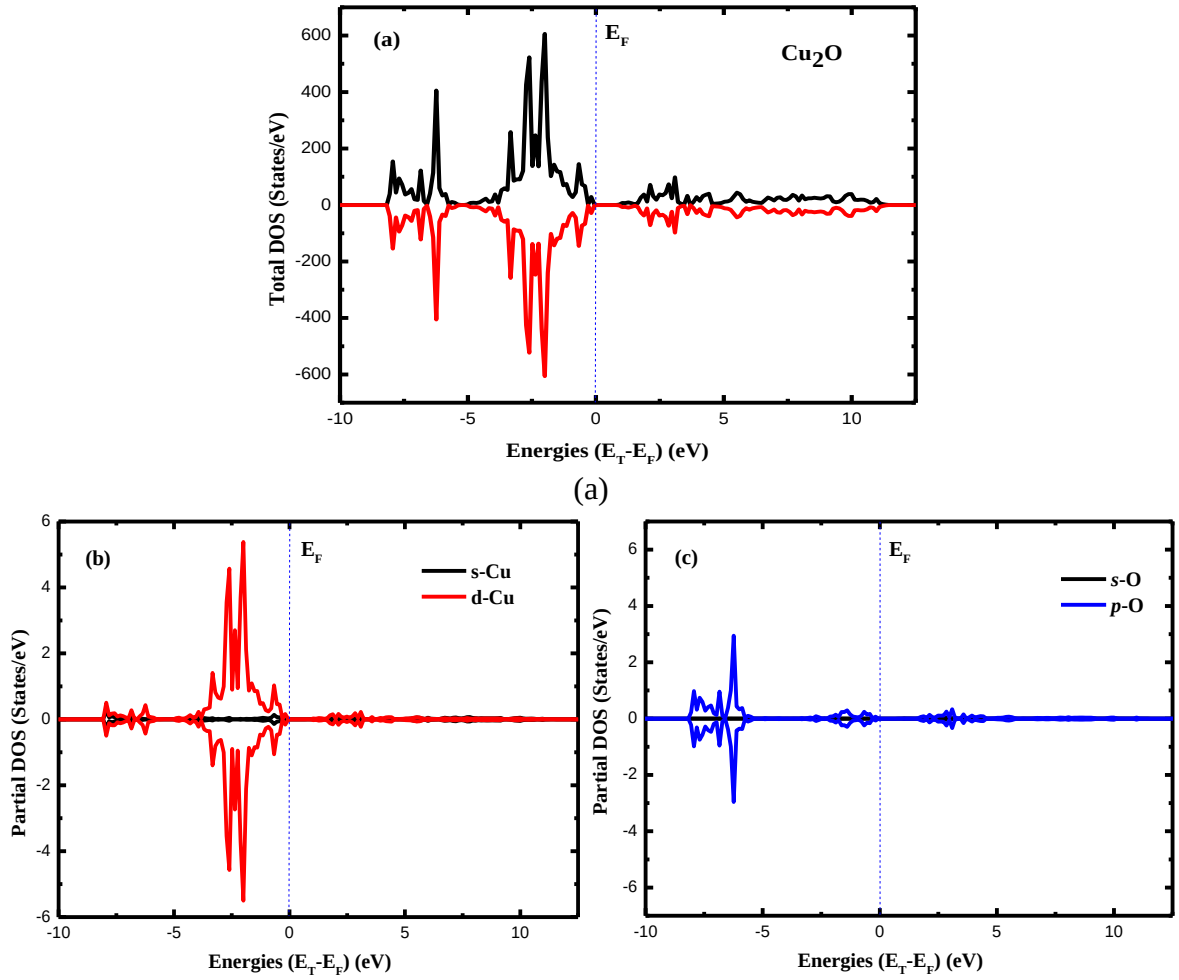

(a) (b) (c)

Fig. 6. Calculated density of states of pure Cu_2O: (a) Total DOS; (b) Partial DOS for Cu; (c) Partial DOS for O. Dashed line is the Fermi level E_F

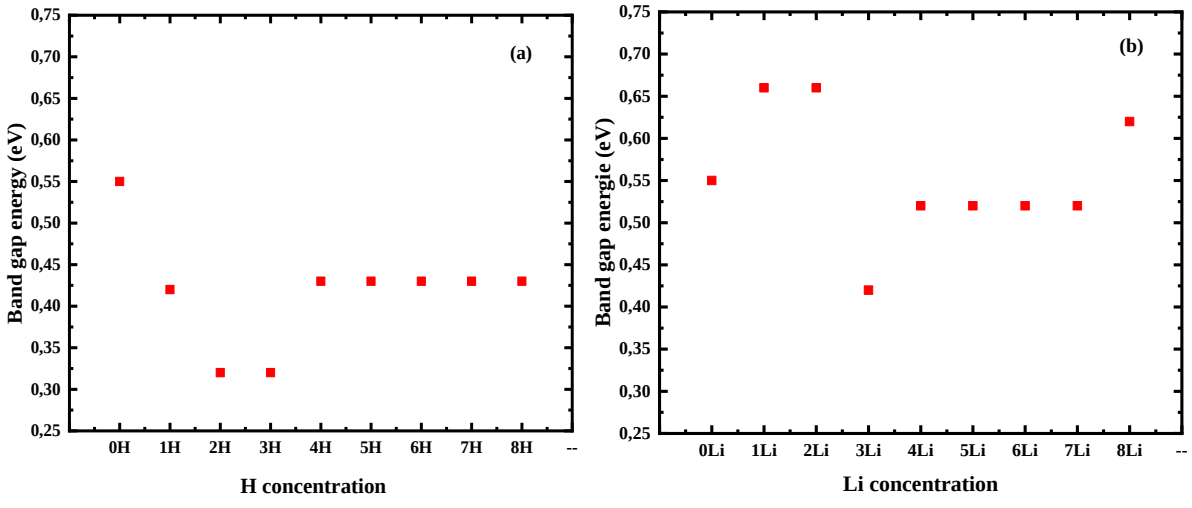

(a) (b)

Fig. 7. Calculated bandgap variation with hydrogen (a) and lithium (b) concentrations

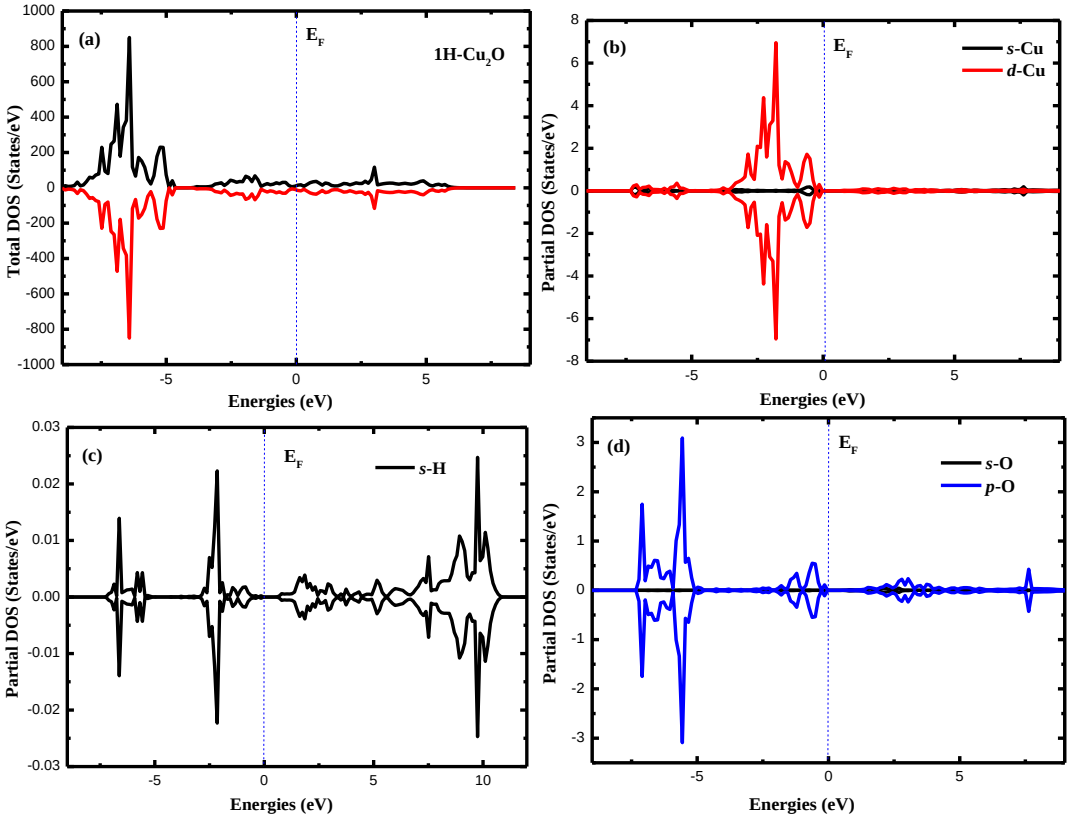

Fig. 8. Calculated density of states of 1H-Cu_2O, (a) Total DOS; (b) Partial DOS for Cu; (c) Partial DOS for H. (d) Partial DOS for O. Dashed line is the Fermi level E_F

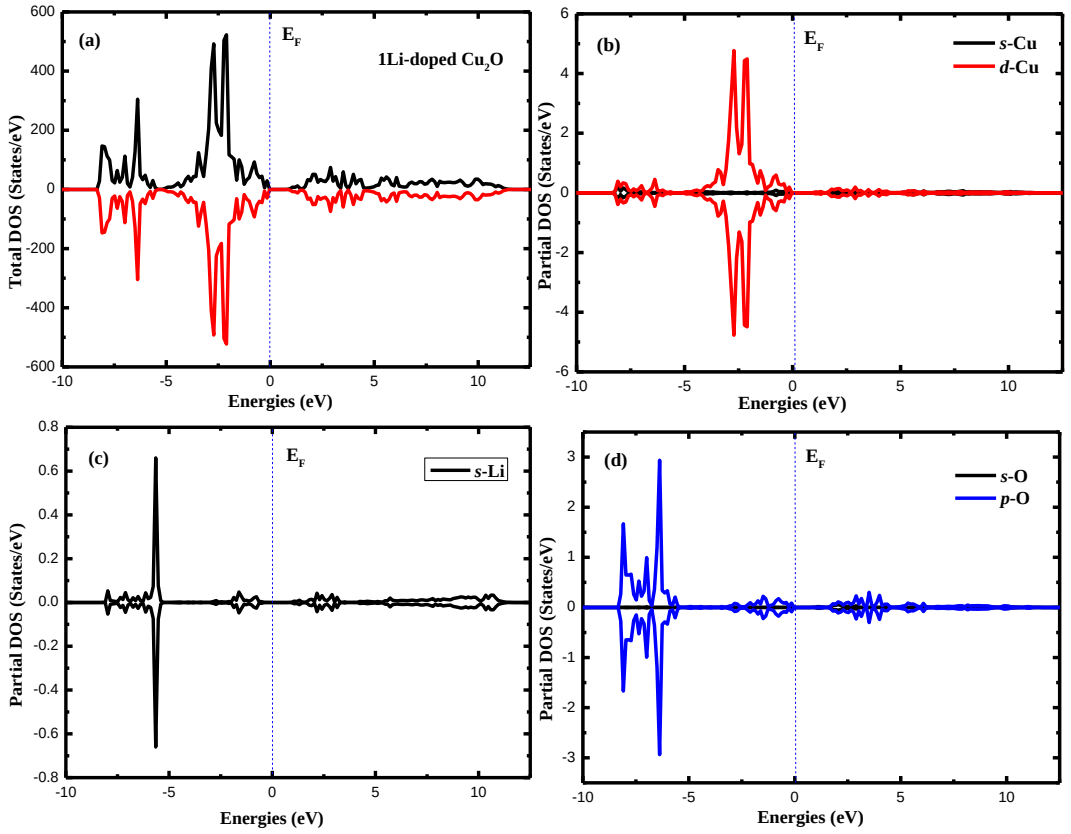

Fig. 9. Calculated density of states of 1Li-Cu_2O, (a) Total DOS; (b) Partial DOS for Cu; (c) Partial DOS for Li. (d) Partial DOS for O. Dashed line is the Fermi level E_F

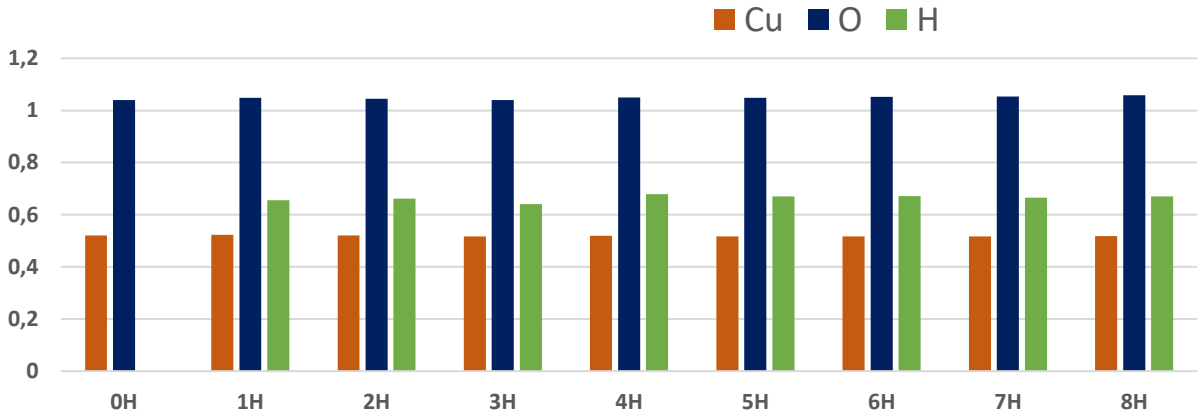

(a)

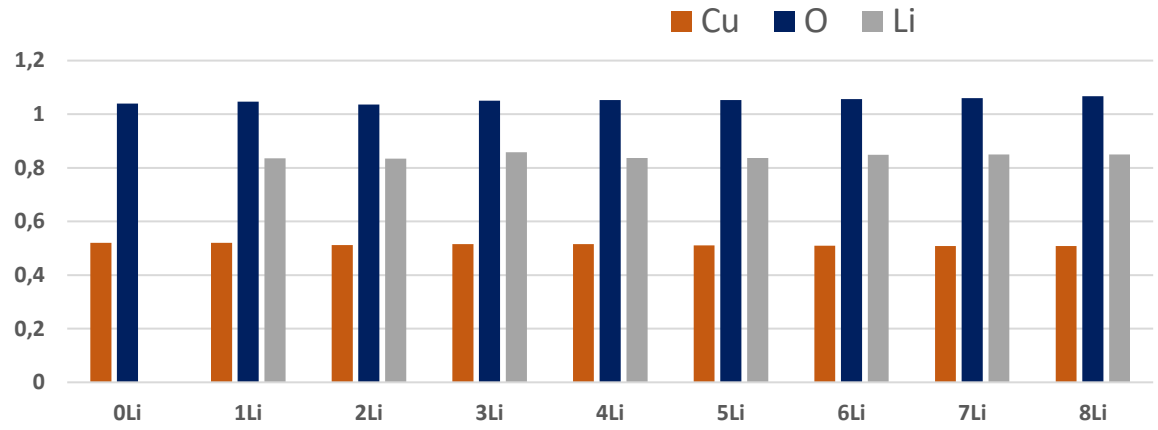

(b)

Fig. 10. Average atomic Bader charges (|e|) on undoped (a), H- and Li-doped (b) Cu_2O

Optical properties

The Cuprous oxide Cu_2O is a material with a low absorption coefficient which means more transmitted light and a promising p-type TCO, but its optical transmittance in the visible spectrum is limited by its relatively low band gap (2.17 eV) [35]. In this paper, we aim at increasing this value with different concentration of hydrogen or lithium.

In Fig. 11, we present the absorption coefficients (in order of 10^5 cm^{-1}) versus the wavelength (nm) of all configurations of H-doped Cu_2O compared to the pure one in the visible light region (400-900 nm) and UV region (250-400 nm). The absorption coefficient of pure Cu_2O can be separated in two regions. The first region, between 250 and 400 nm, where α decreases from 1.815×10^5 cm^{-1} to 0.91×10^5 cm^{-1} and the second one (400-900 nm) in which the absorbance continues to decrease to 0.09×10^5, which is in agreement with experimental results [41,42]. The incorporation of hydrogen decreases the absorbance of pure Cu_2O in the two regions. Additionally, the absorbance is significantly decreased in the visible region for low concentration of hydrogen into Cu_2O; while for the high concentration, the absorbance is almost zero in the 400–900 nm region. We remark a small peak at 650 nm when we doped with H, which is largely influenced by decreasing doping levels. The presence of hydrogen atoms increases the transmittance of Cu_2O.

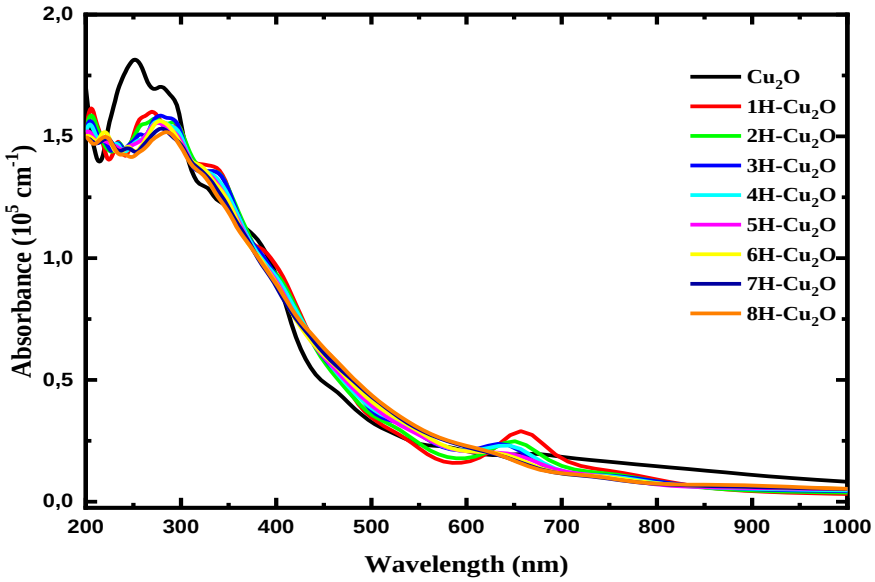

Fig. 11. The variation of the absorption coefficient of l, 2, 3, 4, 5, 6, 7 and 8 H implanted in Cu_2O compared with pure one

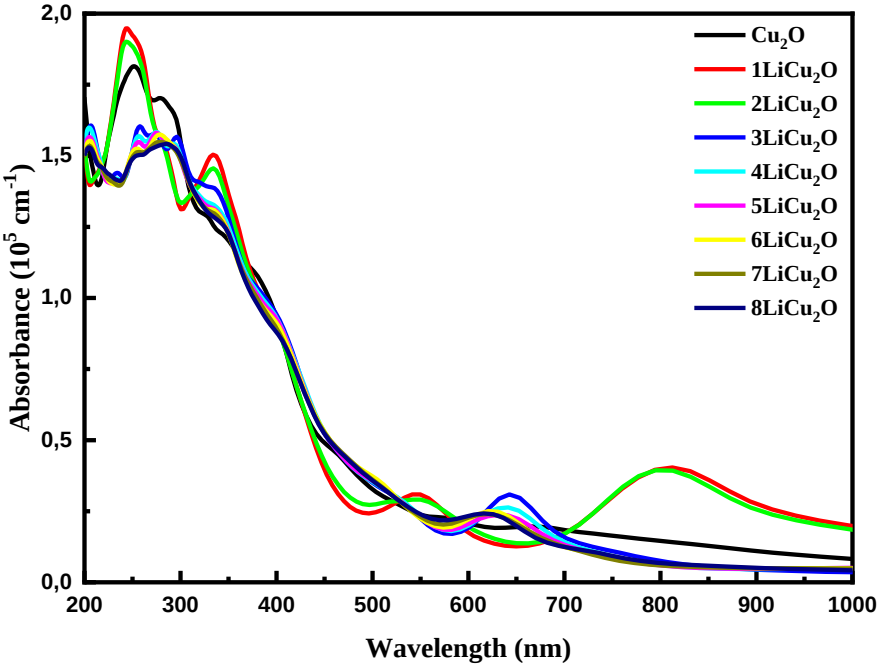

Fig. 12. The variation of the absorption coefficient of l, 2, 3, 4, 5, 6, 7 and 8 Li inserted in Cu_2O compared with pure one

Figure 12 shows the absorption coefficient versus the wavelength (nm) of all configurations of Li-doped Cu_2O compared to the pure one in the visible and UV region. A small change was observed between different concentrations when the Li atom is inserted in the pure Cu_2O. We remark, in the visible region, the presence of two peaks (at 550 and 800 nm) observed in the low concentration of Lithium (1 and 2 atoms) and one peak (at 650 nm) in the high concentration. One notes that with the incorporation of 1 or 2 atoms of Lithium, the absorbance of pure Cu_2O increases in the 250-300 nm region and decreases in the rest of the UV region. The study of Nyborg & al. found that there is an increase of absorption in the case

of Li doping in Cu_2O [14]. Moreover, in the visible region, the absorbance increases when the concentration of Lithium insertion decreases.

Conclusion

In this study, the electronic, magnetic and optical properties are obtained for Cu_2O with hydrogen and lithium. The physical properties of Cu_2O change depending on the concentrations and the inserted element. The optimized lattice constant of Cu_2O is in good agreement with experimental value. The calculated formation energy of different concentrations of H or Li is negative, indicating the stability of the system. The H atom is tightly bound to the adjacent O ion through the O-H bond. The Cu-Li and O-Li bond lengths are slightly reduced. The presence of replacement hydrogen or lithium will not produce a magnetic moment sequence in Cu_2O. Moreover, according to the Fermi level energies the doping system is a degenerate p-type semiconductor. The metal-metal interaction governs the valence and conduction band edges, where the strength of a covalent bond Cu-Cu increased with doping that decreased the band gap energy. For low lithium doping, the optical properties of Cu_2O are improved in the visible light range. On the other hand, when hydrogen is introduced into the Cu_2O structure, its absorbance in the visible light region will sharply increase. This material (H- or Li-Cu_2O) can open several technical leaflets in terms of solar energy conversion and electricity storage and/or hydrogen production and/or storage and other applications.

References

1. Ramanathan S. (Ed.) *Thin Film Metal-Oxides*. NY: Springer; 2010.
2. Xu J, Xue D. Five Branching Growth Patterns in the Cubic Crystal System: A Direct Observation of Cuprous Oxide Microcrystals. *Acta Mater*. 2007;55(7): 2397–2406.
3. Yuhas BD, Yang P. Nanowire-Based All-Oxide Solar Cells. *J. Am. Chem. Soc*. 2009;131(10): 3756–3761.
4. Kale SN, Ogale SB, Shinde SR, Sahasrabuddhe M, Kulkarni VN, Greene RL, Venkatesan T. Magnetism in cobalt-doped Cu2O thin films without and with Al, V, or Zn codopants. *Appl. Phys. Lett*. 2003;82(13): 2100–21002.
5. Miyake M, Chen YC, Braun PV, Wiltzius P. Fabrication of three-dimensional photonic crystals using muitibeam interference lithography and electrodeposition. *Adv. Mater*. 2009;21(29): 3012–3015.
6. Han F, Li D, Li WC, Lei C, Sun Q, Lu AH. Nanoengineered Polypyrrole-Coated Fe2O3@C Multifunctional Composites with an Improved Cycle Stability as Lithium-Ion Anodes. *Adv. Funct. Mater*. 2013;23(13): 1692–1700.
7. Lou P, Cui Z, Jia Z, Sun J, Tan Y, Guo X. Monodispersed Carbon-Coated Cubic NiP2 Nanoparticles Anchored on Carbon Nanotubes as Ultra-Long-Life Anodes for Reversible Lithium Storage. *ACS Nano*. 2017;11(4): 3705–3715.
8. Wang C, Wu L, Wang H, Zuo W, Li Y, Liu J. Fabrication and Shell Optimization of Synergistic TiO2-MoO3 Core–Shell Nanowire Array Anode for High Energy and Power Density Lithium-Ion Batteries. *Adv. Funct. Mater*. 2015;25(23): 3524–3533.
9. Inguanta R, Piazza S, Sunseri C, Template electrosynthesis of aligned Cu2O nanowires: Part I. Fabrication and characterization. *Electrochimica Acta*. 2008;53(22): 6504–6512.
10. Zhang CQ, Tu JP, Huang XH, Yuan YF, Chen XT, Mao F. Preparation and electrochemical performances of cubic shape Cu2O as anode material for lithium ion batteries. *J. Alloys Compd*. 2007;441(1-2): 52–56.
11. Lv Q, Li L, Li Y, Mao J, Chen T, Shao D, Li M, Tan R, Zhao J, Shi S, Wang H, Liu L, Li L. A DFT Study of Electronic Structures and Photocatalytic Properties of Mn–Cu2O. *Russ. J. Phys. Chem. A*. 2020;94: 641–646.

12. Maurya V, Joshi K B, Band structure and thermoelectric properties of Cu2O from GGA and GGA+U approaches. *Bull. Mater. Sci*. 2019;42: 261.
13. Benaissa M, Si Abdelkader H, Merad G. Electronic and optical properties of halogen (H= F, Cl, Br)-doped Cu2O by hybrid density functional simulations. *Optik*. 2020;207: 164440.
14. Nyborg M, Azarov A, Bergum K, Monakhov E. Deposition and characterization of lithium doped direct current magnetron sputtered Cu2O films. *Thin Solid Films*. 2021;722: 138573.
15. Nyborg M, Karlsen K, Bergum K and Monakhov E, Dominant acceptors in Li doped, magnetron deposited Cu2O films. *Mater. Res. Express*. 2021;8(12): 125903.
16. Cai Y, Qin B, Li C, Si X, Cao J, Zheng X, Qiao L, Qi J. A successive "conversion deposition" mechanism achieved by micro-crystalline Cu2O modified current collector for composite lithium anode. *Journal of Industrial and Engineering Chemistry*. 2023;120: 285– 292.
17. Zhang N, Zhao T, Wei L, Feng T, Wu F, Chen R. Stable Li/Cu2O composite anodes enabled by a 3D conductive skeleton with lithiophilic nanowire array. *Journal of Power Sources*. 2022;536: 231374.
18. Zhou X, Fu B, Li L, Tian Z, Xu X, Wu Z, Yang J. Hydrogen-substituted graphdiyne encapsulated cuprous oxide photocathode for efficient and stable photo electrochemical water reduction. *Nat. Commun*. 2022;13: 5770.
19. Chen M, Wang Y, Zhang Y, Yuan Y, Liu J, Liu B, Du Q, Ren Y, Yang H. Hydrogenated Cu2O octahededrons with exposed {111} facets: Enhancing sensing performance and sensing mechanism of 1-coordinated Cu atom as a reactive center. *Sensors and Actuators B: Chemical*. 2020;310: 127827.
20. Kresse G, Furthmüller J. Efficient iterative schemes for ab initio total-energy calculations using a plane-wave basis set. *Phys. Rev. B*. 1996;54(16): 11169.
21. Kresse G, Joubert D. From ultrasoft pseudopotentials to the projector augmented-wave method. *Phys. Rev. B*. 1996;59(3): 1758.
22. Perdew JP, Burke K, Ernzerhof M. Generalized Gradient Approximation Made Simple. *Phys. Rev. Lett*. 1997;77(18): 3865.
23. Blochl PE. Projector augmented-wave method. *Phys. Rev. B*. 1994;50: 17953.
24. Hallberg J, Hanson RC. The elastic constants of cuprous oxide. *Phys. Status Solidi B*. 1970;42: 305–310.
25. Manghnani MH, Brower WS, Parker HS. Anomalous elastic behavior in Cu2O under pressure. *Phys. Status Solidi A*. 1974;25: 69–76.
26. Korzhavyi PA, Johansson B. *Literature review on the properties of cuprous oxide Cu2O and the process of copper oxidation*. 2011.
27. Laskowski R, Blaha P, Schwarz K. Charge Distribution and Chemical Bonding in Cu2O. *Phys. Rev. B*. 2003;67: 075102.
28. Zheng C, Tao Y, Cao JZ, Chen RF, Zhao P, Wu XJ, Huang W. The structural, electronic, and optical properties of ladder-type polyheterofluorenes: a theoretical study. *J. Mol. Model*. 2012;18: 4929.
29. Reshak AH, Auluck S. Calculated optical properties of 2H−MoS2 intercalated with lithium. *Phys. Rev. B*. 2003;68: 125101.
30. Melrose DB, Stoneham RJ. Generalised Kramers-Kronig formula for spatially dispersive media. *J. Phys. A: Math*. 1977;10(1): L17.
31. Van de Walle CG, Denteneer PJH, Bar-Yam Y, Pantelides ST. Theory of hydrogen diffusion and reactions in crystalline silicon. *Phys. Rev. B*. 1989;39(15): 10791.
32. Neugebauer J, Van de Walle CG. Theory of hydrogen in GaN. In: Nickel NH. (ed.) *Hydrogen in Semiconductors II, Semiconductors and Semimetals*. Boston: Academic Press: 1999. p.479–502.

33. Kiran GK, Periyasamy G, Kamath PV. Role of alloying in Cu2O conversion anode for Li-ion batteries. *Theor. Chem. Acc*. 2019;138: 23.
34. Luo Z, Fu L, Zhu J, Yang W, Li D, Zhou L. Cu2O as a promising cathode with high specific capacity for thermal battery. *Journal of Power Sources*. 2020;448: 227569.
35. Kittel C. *Introduction to Solid State Physics*. 6th Ed. New York: Wiley; 1986.
36. Marksteiner P, Blaha P, Schwarz K. Electronic structure and binding mechanism of Cu2O. *Z. Physik B - Condensed Matter*. 1986;64: 119–127.
37. Martnez-Ruiz A, Moreno M G, Takeuchi N. First Principles Calculations of the Electronic Properties of Bulk Cu2O, Clean and Doped with Ag, Ni, and Zn. *Solid State. Sci.* 2003;5(2): 291–295.
38. Soon A, Todorova M, Delley B, Stampfl C. Oxygen adsorption and stability of surface oxides on Cu(111): A first-principles investigation. *Phys. Rev. B*. 2006;73(16): 165424.
39. Islam MM, Diawara B, Maurice V, Marcus P. Bulk and surface properties of Cu2O: A first-principles investigation. *J. Mol. Struc.: THEOCHEM*. 2009;903(1-3): 41–48.
40. Janotti A, Van de Walle CG. Hydrogen multicentre bonds. *Nature Mater*. 2007;6(1): 44–47.
41. Luo Yu, Liangbin Xiong, and Ying Yu, Cu2O Homojunction Solar Cells: F-Doped N-type Thin Film and Highly Improved Efficiency. *J. Phys. Chem. C*. 2015;119(40): 22803−22811.
42. Zhong D. Synergetic effects of Cu2O photocatalyst with titania and enhanced photoactivity under visible irradiation. *Acta Chimica Slovaca*. 2013;6(1): 141–149.

THE AUTHORS

Amina Larabi
e-mail: Larabi.Amina@crtse.dz

Mourad Mebarki
e-mail: Mebarki.Mourad@crtse.dz

Ibrahim Abdellaoui
e-mail**:** abdellaoui.ibrahim@yahoo.fr

Ammaria Mahmoudi
e-mail: amaria_physique@yahoo.fr

Saloua Merazga
e-mail: Merazga.Saloua@crtse.dz

Noureddine Gabouze
e-mail: gabouzenoureddine@crtse.dz